



Fermi National Accelerator Laboratory

FERMILAB-Conf-97/152-E

CDF and DØ

W+ Jets Production at the Fermilab Tevatron

Jay R. Dittmann

For the CDF and DØ Collaborations

Duke University

Durham, North Carolina 27708-0305

Fermi National Accelerator Laboratory

P.O. Box 500, Batavia, Illinois 60510

May 1997

Published Proceedings of the *QCD and High Energy Hadronic Interactions, XXXII Rencontres de Moriond*, Les Arcs, France, March 22-29, 1997

Disclaimer

This report was prepared as an account of work sponsored by an agency of the United States Government. Neither the United States Government nor any agency thereof, nor any of their employees, makes any warranty, expressed or implied, or assumes any legal liability or responsibility for the accuracy, completeness, or usefulness of any information, apparatus, product, or process disclosed, or represents that its use would not infringe privately owned rights. Reference herein to any specific commercial product, process, or service by trade name, trademark, manufacturer, or otherwise, does not necessarily constitute or imply its endorsement, recommendation, or favoring by the United States Government or any agency thereof. The views and opinions of authors expressed herein do not necessarily state or reflect those of the United States Government or any agency thereof.

Distribution

Approved for public release; further dissemination unlimited.

May 21, 1997

W + JETS PRODUCTION AT THE FERMILAB TEVATRON

Jay R. Dittmann
Duke University
Durham, NC 27708-0305, USA

For the CDF and D0 Collaborations

Abstract

The production properties of jets in W events have been measured using $\sqrt{s} = 1.8$ TeV $p\bar{p}$ collisions at the Fermilab Tevatron Collider. Experimental results from several CDF and D0 analyses are compared to leading-order and next-to-leading-order QCD predictions.

*To appear in
Proceedings of the XXXII Rencontres de Moriond
QCD and High Energy Hadronic Interactions*

Introduction

The Fermilab Tevatron Collider has provided a large sample of W boson events with hadronic jets from $\sqrt{s} = 1.8$ TeV $p\bar{p}$ collisions. These data allow a variety of valuable tests of leading-order (LO) and next-to-leading-order (NLO) QCD. This paper compares measurements in W events to QCD predictions for three different analyses: (1) production properties of W + jets events at CDF, (2) measurement of the $(W + 1 \text{ jet}) / (W + 0 \text{ jet})$ cross section ratio at D0, and (3) color coherence in W events at D0.

1 Production Properties of W + Jets Events at CDF

This analysis compares the properties of hadronic jets in W events to leading-order QCD predictions of direct single W production with added initial and final state radiation. Measurements of $W + \geq n$ jet cross sections ($n = 1$ to 4) and kinematical distributions are used to test QCD and probe for physics beyond the Standard Model.

Using 108 pb^{-1} of Run 1A + 1B data at CDF, $W^\pm \rightarrow e^\pm \nu$ candidates are selected from events that pass the online trigger¹ by requiring missing transverse energy $\cancel{E}_T > 30$ GeV and a clean² central electron with transverse energy $E_T > 20$ GeV. Jets are clustered using a cone algorithm³ with cone size 0.4 in η - ϕ space. After correcting for calorimeter non-uniformities, out-of-cone energy, and underlying event contributions, jets are selected with $E_T > 15$ GeV and $|\eta| < 2.4$. Of the 51431 $W \rightarrow e\nu$ candidates, 11144 have ≥ 1 jets, 2596 have ≥ 2 jets, 580 have ≥ 3 jets, 126 have ≥ 4 jets, and 21 have ≥ 5 jets.

The W boson background is dominated by QCD multijet production in which a jet fakes an electron and mismeasured jet energies result in large \cancel{E}_T . This background varies from 3–27% for jet multiplicity $n \geq 0$ to 4. Smaller backgrounds from $W \rightarrow \tau\nu$ (with $\tau \rightarrow e\nu\bar{\nu}$), $Z \rightarrow \tau\tau$, and $Z \rightarrow ee$ total 3% at each jet multiplicity. Contributions of true $W \rightarrow e\nu$ decays from Standard Model top production range from 0.1–26% for $n \geq 0$ to 4 and are removed to yield measurements of direct single W production. Although contributions from WW and WZ are negligible, a small correction is made for $W\gamma$ events in which the photon is counted as a jet. Jet multiplicities are also corrected by 3–10% for jets produced in other $p\bar{p}$ interactions. The overall $W \rightarrow e\nu$ detection efficiencies, which are $\approx 20\%$ for each jet multiplicity, account for the online trigger, fiducial and kinematic acceptances, electron ID cuts, and jets that overlap electrons.

$W + \geq n$ jet cross sections are obtained by measuring ratios of the number of $\geq n$ to ≥ 0 jet events (corrected for backgrounds and efficiencies), and multiplying by a previous CDF inclusive $W \rightarrow e\nu$ cross section measurement of $2490 \pm 120 \text{ pb}$.⁴ The measured cross sections are compared to QCD predictions generated using the VECBOS⁵ Monte Carlo based on $W + n$ parton matrix elements for $n = 1$ to 4. Initial state gluon radiation, final state parton fragmentation, and hadronization are included using the HERWIG⁶ shower simulation algorithm. HERWIG provides a partial higher-order correction to the VECBOS tree-level diagrams. Its output, when processed through the CDF detector simulation, yields jets that are clustered and corrected like jets in the data.

Fig. 1(a) compares the measured $W + \geq n$ jet cross sections to QCD predictions calculated using the CTEQ3M⁷ parton density functions at two different renormalization

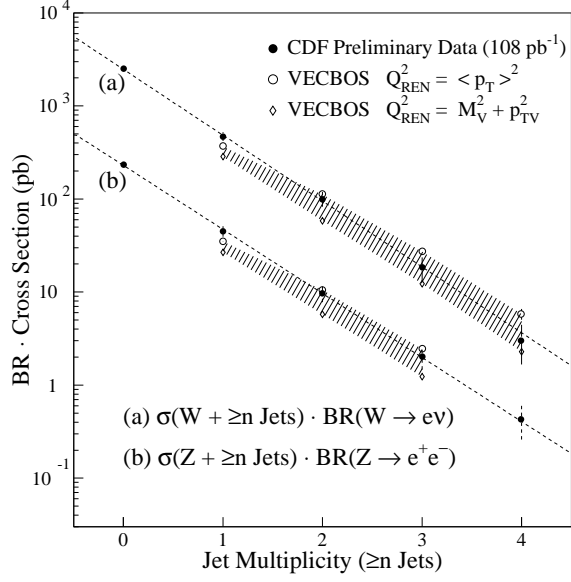


Fig. 1: Cross sections for (a) $W + \geq n$ jets and (b) $Z + \geq n$ jets for $n = 0$ to 4. The LO QCD prediction bands span the range of renormalization scales described in the text. The error bars include both statistical and systematic uncertainties and the lines are exponential fits to the data.

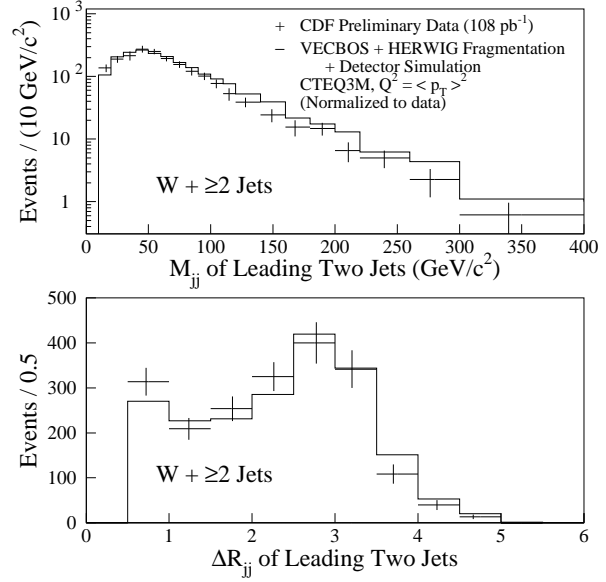


Fig. 2: (a) Invariant mass (M_{jj}) and (b) separation in $\eta - \phi$ space (ΔR_{jj}) of the two highest- E_T jets in $W + \geq 2$ jet events. The QCD predictions are normalized to the data. The error bars include statistical uncertainties and background subtraction systematics.

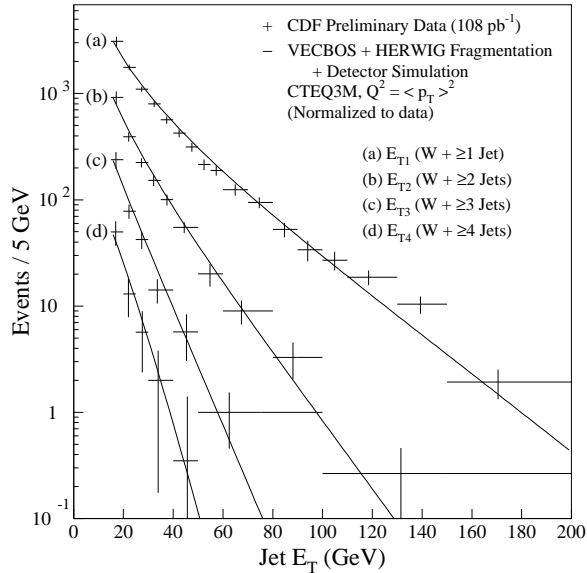


Fig. 3: E_T of the (a) first, (b) second, (c) third, and (d) fourth jets (ordered by decreasing E_T) in ≥ 1 , ≥ 2 , ≥ 3 , and ≥ 4 jet events, respectively. The curves represent LO QCD predictions for $Q^2 = \langle p_T \rangle^2$, normalized to the data. The error bars include statistical uncertainties and background subtraction systematics.

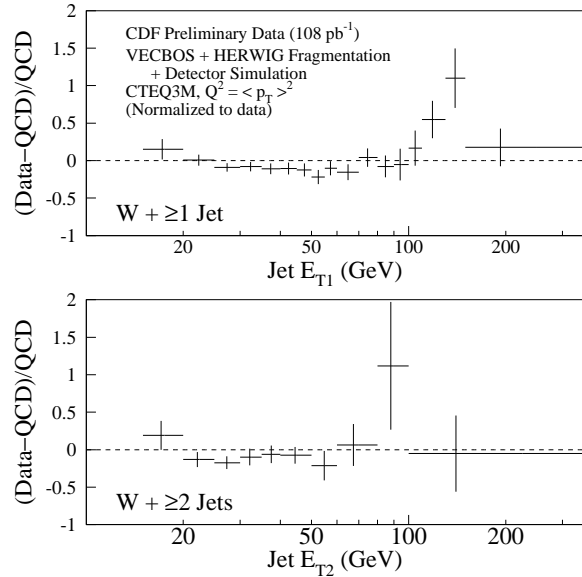


Fig. 4: Distributions of $(\text{Data}-\text{QCD})/\text{QCD}$ with $Q^2 = \langle p_T \rangle^2$ for (a) E_{T1} in $W + \geq 1$ jet events and (b) E_{T2} in $W + \geq 2$ jet events. The QCD prediction is normalized to the data to permit a shape comparison. The error bars include statistical uncertainties and background subtraction systematics.

scales: $Q^2 = M_W^2 + p_{T_W}^2$ of the boson, and $Q^2 = \langle p_T \rangle^2$ of the partons. The harder scale ($M_W^2 + p_{T_W}^2$) predicts relative cross sections that are smaller in magnitude by a factor of 1.7 for each n . The predictions for $Q^2 = \langle p_T \rangle^2$ are 1.3 times lower for ≥ 1 jets, but exceed the data for ≥ 2 to ≥ 4 jets. Thus, within the inherent uncertainty of the LO calculation, the predicted and measured $W + \geq n$ jet cross sections agree for $n = 2$ to 4. Similar behavior is observed in Fig. 1(b) for QCD predictions of $Z \rightarrow e^+e^- +$ jets cross sections.⁸

The QCD predictions are also tested using jet kinematic properties. The invariant mass (M_{jj}) and separation (ΔR_{jj}) of the two highest- E_T jets in $W + \geq 2$ jet events are compared to QCD predictions ($Q^2 = \langle p_T \rangle^2$) in Fig. 2. The measured and predicted jet E_T spectra for jets 1–4 (ordered by decreasing E_T) are shown in Fig. 3. Distributions of (Data–QCD)/QCD for E_{T1} and E_{T2} are shown in Fig. 4. The plots show that the data and QCD predictions agree reasonably well, although the high statistics of the $W + \geq 1$ jet sample reveal the limitation of this QCD approximation for low E_T (< 20 GeV) and high E_T (> 100 GeV) jets. These regions rely heavily upon the HERWIG partial higher-order corrections. At low E_T , initial state gluon radiation is sometimes hard enough to replace the parton generated in the LO matrix element. At high E_T , over 50% of the $W + \geq 1$ jet data events have ≥ 2 jets, which explicitly indicates the need for higher order corrections to the $W + 1$ parton calculation.

2 Measurement of the ($W + 1$ Jet) / ($W + 0$ Jet) Cross Section Ratio at D0

This analysis measures the ratio of $W + 1$ jet to $W + 0$ jet cross sections (\mathcal{R}^{10}) using $W^\pm \rightarrow e^\pm \nu$ events. Based on a previous D0 study,⁹ this measurement uses a larger data sample (78 pb⁻¹) collected during the 1994–95 Tevatron run.

$W \rightarrow e\nu$ candidates are selected from events that pass the D0 online trigger¹⁰ by requiring $\cancel{E}_T > 25$ GeV and a high quality central electron with $E_T > 25$ GeV. Jets are identified in these events using a fixed cone algorithm with a radius of 0.7 in η - ϕ space. A minimum jet E_T cut (E_T^{min}) of 25 GeV yields 2841 $W + 1$ jet candidates and 33511 $W + 0$ jet candidates. Backgrounds from multijet events, the largest source, are estimated using data to be 6.8% (1.6%) for one (zero) jet events. Smaller backgrounds from Drell-Yan, $Z \rightarrow ee$, and $Z \rightarrow \tau\tau$ are estimated using the ISAJET¹¹ Monte Carlo. After subtracting backgrounds and accounting for electron efficiencies, the final cross section ratio measurement is $\mathcal{R}^{10} = 0.094 \pm 0.004(\text{stat}) \pm 0.008(\text{syst})$ for $E_T^{min} = 25$ GeV. The jet energy scale uncertainty dominates the systematics.

Measurements of \mathcal{R}^{10} for various values of E_T^{min} are shown in Fig. 5, compared to NLO QCD calculations generated using the DYRAD¹² Monte Carlo with renormalization scale $\mu^2 = M_W^2$ for two different parton density functions (PDFs): MRSA¹³ and CTEQ4M.¹⁴ The predictions for both PDFs describe the shape of the E_T^{min} dependence observed in the data, but are significantly smaller in size. Fig. 6 shows the calculated values of \mathcal{R}^{10} ($E_T^{min} = 25$ GeV) for both PDFs, refit for several fixed values of α_s . Not only are the predictions consistently less than the experimental measurement, but they also exhibit little dependence on α_s , making an extraction of α_s by this method impossible.

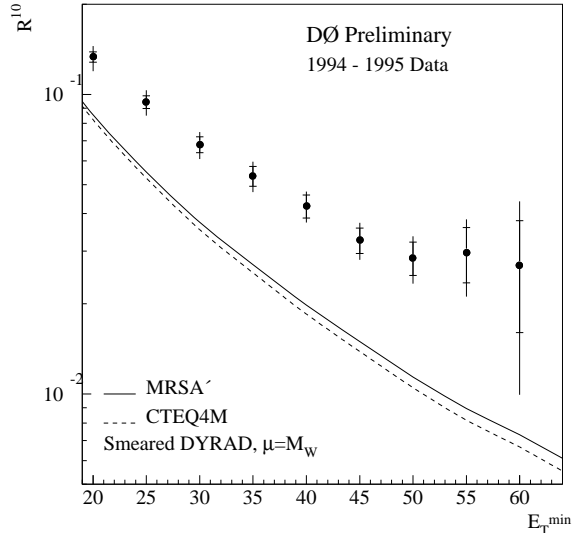


Fig. 5: Measurement of \mathcal{R}^{10} as a function of E_T^{\min} , compared to DYRAD NLO QCD predictions ($\mu^2 = M_W^2$) for MRSA' and CTEQ4M. Detector effects are simulated in the predictions. The inner error bars include statistical uncertainties; the outer error bars include statistical and systematic uncertainties in quadrature.

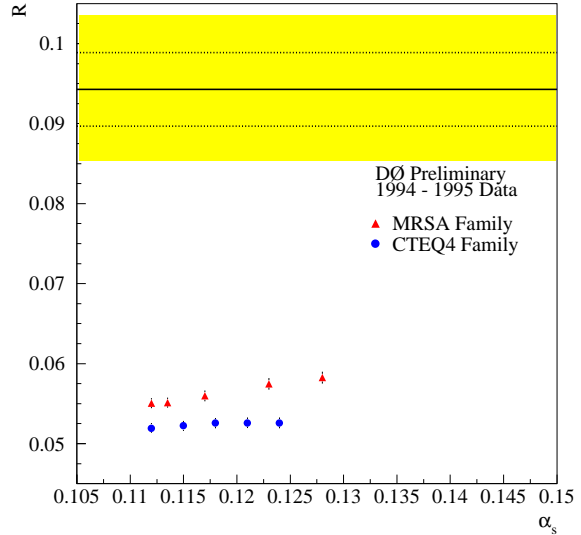


Fig. 6: Measurement of \mathcal{R}^{10} at $E_T^{\min} = 25$ GeV compared to smeared DYRAD NLO QCD predictions ($\mu^2 = M_W^2$) for two different PDF families, refit for various values of α_s . The experimental result is the solid line. Dotted lines indicate the statistical uncertainty, and the shaded region represents statistical and systematic uncertainties added in quadrature.

3 Observation of Color Coherence in W Events at D0

In perturbative QCD, color coherence effects arise from the interference of soft gluon radiation emitted along color-connected partons. This D0 analysis uses $W^\pm \rightarrow e^\pm \nu$ + jet events to explore initial-to-final state coherence effects in $p\bar{p}$ interactions by comparing the pattern of soft particle flow around the jet to that measured in the direction of the colorless W boson.

$W \rightarrow e\nu$ events with jets are selected using cuts like those of the \mathcal{R}^{10} analysis with two extra requirements: a W with rapidity $y < 0.7$, and a jet with $|\eta| < 0.7$ opposite the W ($\pi/2 < \Delta\phi < 3\pi/2$). Annuli are defined in the directions of the W and jet in these events (see Fig. 7), and the number of calorimeter towers N with $E_T > 250$ MeV is measured in each annulus as a function of $\beta = \arctan(\text{sign}(\eta)\Delta\phi/\Delta\eta)$. To improve statistics, the annuli are folded about the ϕ symmetry axis into the β range $0-\pi$.

Color coherence effects are expected to produce larger tower multiplicities around the jet in the “near beam” ($\beta = 0$) and “far beam” ($\beta = \pi$) directions. Measuring N_{Jet}/N_W versus β tests this prediction and allows many systematics to cancel in the ratio.

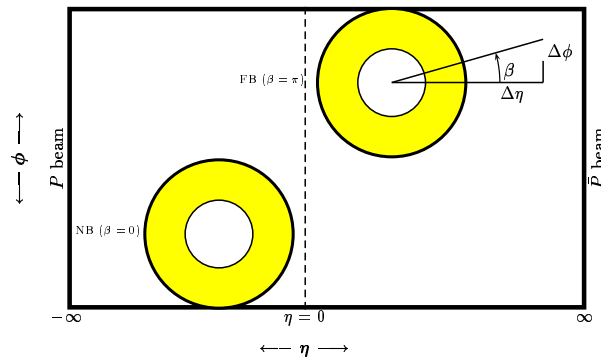


Fig. 7: Calorimeter view for the D0 analysis of color coherence in $W \rightarrow e\nu$ events. Two annuli (each with inner radius $R = 0.7$ and outer radius $R = 1.5$) are defined in the directions of the W and jet. β is defined as $\arctan(\text{sign}(\eta)\Delta\phi/\Delta\eta)$.

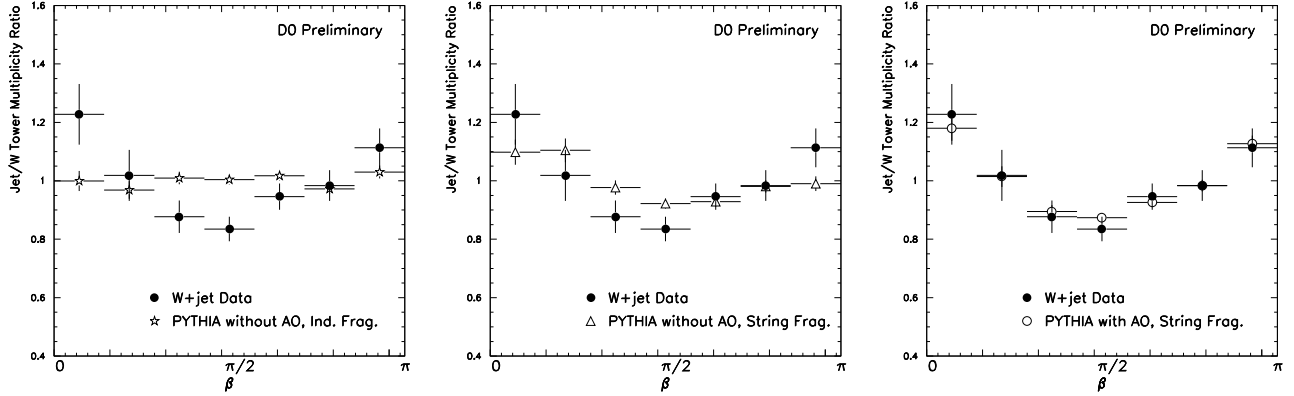


Fig. 8: Tower multiplicity ratio N_{Jet}/N_W vs. β for W data, compared to PYTHIA using three different implementations of angular ordering (AO) and fragmentation. Detector effects are simulated in the predictions. All distributions are normalized to unity to permit shape comparisons.

The W data are compared to QCD predictions generated using PYTHIA v5.7.¹⁵ PYTHIA incorporates color coherence effects using angular ordering and string fragmentation, each of which can be turned on independently. Fig. 8 compares the measured ratio N_{Jet}/N_W vs. β to PYTHIA for three different implementations of angular ordering and fragmentation. The high level of agreement between data and PYTHIA when coherence effects are turned on supports the observation of color coherence in the W data.

Summary

Properties of jets in W events have been compared to QCD predictions in several analyses at the Fermilab Tevatron. CDF has observed good agreement between data and LO QCD in measurements of $W + \geq n$ jet cross sections and jet properties, although the large statistics of the W sample reveal the need for higher-order corrections to the $W + 1$ parton calculation. D0 has observed color coherence as predicted by QCD; however, a measurement of the $(W + 1 \text{ jet}) / (W + 0 \text{ jet})$ cross section ratio reveals a large discrepancy between the data and theoretical predictions.

References

- [1] F. Abe *et al.*, Nucl. Instrum. Methods A **271**, 387 (1988).
- [2] F. Abe *et al.*, Phys. Rev. D **44**, 29 (1991).
- [3] F. Abe *et al.*, Phys. Rev. D **45**, 1448 (1992).
- [4] F. Abe *et al.*, Phys. Rev. Lett. **76**, 3070 (1996).
- [5] F.A. Berends *et al.*, Nucl. Phys. B **357**, 32 (1991).
- [6] G. Marchesini and B. Webber, Nucl. Phys. B **310**, 461 (1988).
- [7] H.L. Lai *et al.*, Phys. Rev. D **51**, 4763 (1995).
- [8] F. Abe *et al.*, Phys. Rev. Lett. **77**, 448 (1996).
- [9] S. Abachi *et al.*, Phys. Rev. Lett. **75**, 3226 (1995).
- [10] S. Abachi *et al.*, Nucl. Instrum. Methods A **338**, 185 (1994).
- [11] F.E. Paige and S.D. Protopopescu, "ISAJET Manual," Brookhaven National Laboratory, Upton, New York (1992).
- [12] W.T. Giele, E.W.N. Glover, and D.A. Kosower, Nucl. Phys. B **403**, 633 (1993).
- [13] A.D. Martin, R.G. Roberts, and W.J. Stirling, Phys. Lett. B **356**, 89 (1995).
- [14] H.L. Lai *et al.*, Phys. Rev. D **55**, 1280 (1997).
- [15] T. Sjöstrand, Comput. Phys. Commun. **82**, 74 (1994).